# Numerical Simulation of the Overrolling of a Surface Feature in an EHL Line Contact

**C. H. Venner**
University of Twente,
Enschede, The Netherlands

**A. A. Lubrecht**
SKF Engineering & Research Centre B.V.,
Nieuwegein, The Netherlands

**W. E. ten Napel**
University of Twente,
Enschede, The Netherlands

*In this paper a Multigrid extension of a stationary solver is outlined for the EHL solution of a line contact under transient conditions. The solver is applied to calculate pressure and film thickness profiles at each time step when an indentation is moving through the contact, which results in an asymmetric pressure profile. The time-dependent results are compared with the stationary solutions. The pressure as a function of time is presented as well as the integrated pressure (over time) as a function of the spatial coordinate. These time-dependent pressures are used to compute the sub-surface stress field, which shows higher stresses below the trailing edge of the indentation. Therefore the risk of fatigue is higher below the trailing edge of the indentation, as is experimentally observed. The transient pressures can be used for a fundamental study of the emitted frequency spectrum of rolling bearings, as used in condition monitoring.*

## 1 Introduction

Over the last decades the theoretical analysis of elastohydrodynamically lubricated contacts has received much attention in tribological literature. Because of the limitations in available computer resources, classical studies were restricted to the macrogeometry of the contact, i.e., they assumed perfectly smooth surfaces [1,2] and attempts to study the effects of the microgeometry were based on averaged equations, e.g., the flow factor method [3,4]. Because of the constant increase in computer power the total number of calculational points has grown steadily, enabling scientists to model the contacting surfaces more accurately and to study contact features on a micro scale.

However, the analysis of such features introduces the need for a time-dependent approach since both surfaces move in general. An accurate transient analysis requires the solution of the model equations at a large number of time steps. As the computing time needed for each time step is approximately equal to the time required for the solution of the steady state problem, it is obvious that an accurate transient simulation requires a fast algorithm for the solution of the pressure and film shape in the contact. Moreover, to simulate situations of practical importance, that is with a maximum Hertzian pressure of some 2.0 GPa, the algorithm should also be stable.

However, most algorithms for the solution of the steady state line and point contact problem presented over the years are of relatively high complexity. When extended to study transient situations the accuracy that can be obtained is rather limited even when high speed computers are used. Hence, the transient results presented so far have been obtained using a relatively small number of nodes in spatial direction(s) and only a few time steps [5,6,7]. Furthermore, most likely because of stability problems, only relatively lightly loaded situations have been studied. To avoid the aforementioned computational complexities, many papers deal only with the steady state problem.

Recently, Venner et al. [8] presented a fast and stable algorithm for the computation of the pressure distribution and film shape in EHL line contact situations. The algorithm enabled the solution of the steady state problem, even for highly loaded situations with a large number of nodes on a mini computer (HP 9000/800). This algorithm has been extended to solve transient problems, and some results with respect to the overrolling of a surface indentation are presented in this paper. The low complexity of the algorithm enabled a simulation using a relatively large number of nodes in spatial direction combined with a small time step.

The results of the simulation and their implications for the fatigue life of the contact are discussed. It is demonstrated that extrapolation of results from a stationary analysis to practical conditions where the surface feature is moving can be misleading. Furthermore, the relation of the simulation results with the detection of surface defects using vibration analysis in the condition monitoring of bearings is discussed.

## 2 Equations

After substitution of the following dimensionless variables:

$$\bar{\rho} = \rho/\rho_0$$

$$\bar{\eta} = \eta/\eta_0$$

$$X = x/b$$

$$P = p/p_h$$

$$H = hR/b^2$$

$$T = tu_s/(2b)$$

Contributed by the Tribology Division for publication in the JOURNAL OF TRIBOLOGY. Manuscript received by the Tribology Division July 23, 1990. Associate Editor: B. J. Hamrock.

with: $b$ = Hertzian half width:

$$b=\sqrt{\frac{8wR}{\pi E'}}$$

and $p_h$ = maximum Hertzian pressure:

$$p_h=\frac{2w}{\pi b}$$

the one-dimensionless Reynolds equation reads:

$$\frac{d}{dX}\left(\epsilon\frac{dP}{dX}\right)-\frac{d(\bar{\rho}H)}{dX}-\frac{d(\bar{\rho}H)}{dT}=0 \qquad (1)$$

where the cavitation condition $P\geq 0$ should be satisfied in the entire domain, and the boundary conditions are $P=0$.
$\epsilon$ is given by:

$$\epsilon=\frac{\bar{\rho}H^3}{\bar{\eta}\lambda}$$

where

$$\lambda=\frac{6\eta_0 u_s R^2}{b^3 p_h}$$

The dimensionless lubricant density $\bar{\rho}$ is assumed to depend on the pressure according to the Dowson and Higginson relation [1]. Besides, the Roelands viscosity pressure relation is used. It reads:

$$\bar{\eta}=\frac{\eta}{\eta_0}=\exp\left[\frac{\alpha p_0}{z}\left[\left(1+\frac{P}{P_0}\right)^z-1\right]\right] \qquad (2)$$

where $P_0=p_0/p_h$ and $p_0=1.98\ 10^8$ [Pa].

Substitution of the same dimensionless variables in the film thickness equation gives:

$$H(X,T)=H_0(T)+\frac{X^2}{2}+\Re(X,T)-\frac{1}{\pi}\int_{-\infty}^{\infty}P(Y,T)\ln|X-Y|dY \qquad (3)$$

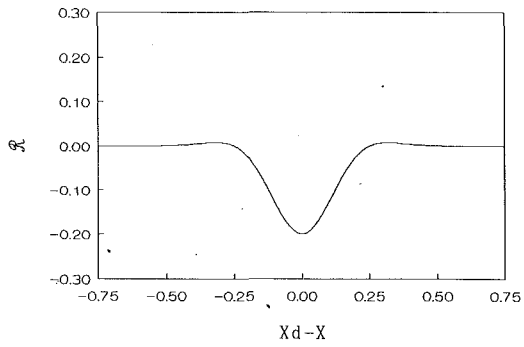


**Fig. 1 Dent geometry**

where: $H_0(T)$ = integration constant determined by the force balance condition.
$\Re(X,T)$ = geometry of surface feature

In the most general situation $\Re(X,T)$ consists of all features on both surfaces that result in a deviation of the undeformed gap from its usual parabolical shape, i.e. surface roughness, surface waviness, bumps, indentations, etc. However, this paper is restricted to the situation of a single indentation on one of the running surfaces moving through the contact. The following dent geometry is assumed, e.g. see Fig. 1:

$$\Re(X,T)=\mathfrak{A}\ 10^{-10\left(\frac{X-X_d}{\mathfrak{W}}\right)^2}\cos\left(2\pi\frac{X-X_d}{\mathfrak{W}}\right) \qquad (4)$$

where: $\mathfrak{A}$ = dimensionless amplitude of the dent
$\mathfrak{W}$ = dimensionless wavelength of the dent
$X_d$ = dimensionless position of the center of the dent at time $T$

This specific shape was preferred over a simple harmonic dent because it models a physical dent more realistically, i.e., it also contains the bulged-out shoulders resulting from the indentation of the material.

The dent is assumed to be located on the surface moving

## Nomenclature

$\mathfrak{A}$ = dimensionless amplitude, $\mathfrak{A}=\frac{aR}{b^2}$
$b$ = half-width Hertzian contact region, $b=\sqrt{\frac{8wR}{\pi E'}}$
$E$ = elasticity modulus (Young's modulus)
$E'$ = reduced modulus of elasticity, $\frac{2}{E'}=\frac{1-\nu_1^2}{E_1}+\frac{1-\nu_2^2}{E_2}$
$G$ = material parameter, $G=\alpha E'$
$h$ = film thickness
$H$ = dimensionless film thickness, $H=\frac{hR}{b^2}$
$H_{0,k}$ = integration constant in dimensionless film thickness equation
$\mathfrak{I}$ = integral of pressure over time
$K_{i,j}^{\Delta_x\Delta_x}$ = discretized kernel in film thickness equation
$L$ = dimensionless material parameter (Moes), $L=G(2U)^{1/4}$
$M$ = dimensionless load parameter (Moes), $M=W(2U)^{-1/2}$
$p$ = pressure
$p_h$ = maximum Hertzian pressure, $p_h=\frac{2w}{\pi b}$
$p_0$ = constant in Roelands' relation
$P$ = dimensionless pressure, $P=\frac{p}{p_h}$
$P_0$ = dimensionless constant, $P_0=\frac{p_0}{p_h}$
$R$ = reduced radius of curvature, $R^{-1}=R_1^{-1}+R_2^{-1}$
$\Re$ = geometry of surface feature
$t$ = time
$T$ = dimensionless time, $T=2tu_s/b$
$u_s$ = sum velocity, $u_s=u_1+u_2$
$U$ = dimensionless speed parameter, $2U=\frac{\eta_0 u_s}{E'R}$
$w$ = load per unit width
$W$ = dimensionless load, $W=\frac{w}{E'R}$
$\mathfrak{W}$ = dimensionless wavelength
$x$ = coordinate
$X$ = dimensionless coordinate, $X=\frac{x}{b}$
$z$ = Roelands' pressure viscosity parameter
$\alpha$ = pressure viscosity index
$\Delta_x$ = distance between two neighboring gridpoints
$\Delta_t$ = time step
$\epsilon$ = coefficient in Reynolds equation, $\epsilon=\frac{\bar{\rho}H^3}{\bar{\eta}\lambda}$
$\lambda$ = dimensionless velocity parameter, $\lambda=6\frac{\eta_0 u_s R^2}{b^3 p_h}$
$\nu$ = Poisson's ratio
$\eta$ = viscosity
$\eta_0$ = viscosity at atmospheric pressure
$\bar{\eta}$ = dimensionless viscosity, $\bar{\eta}=\frac{\eta}{\eta_0}$
$\rho$ = density
$\rho_0$ = density at atmospheric pressure
$\bar{\rho}$ = dimensionless density, $\bar{\rho}=\frac{\rho}{\rho_0}$

with velocity $u_2 = u_s/2$. If the position of the dent $x_d$ at $t=0$ is given by $x_s$ then its location at time $t$ is given by: $x_d = x_s + u_2 t$. Hence, in terms of the dimensionless variables its position at time $T$ is given by:

$$X_d = X_s + 2\frac{u_2}{u_s}T$$

At all times the solution is subject to the condition of force balance, i.e. the integral over the pressure equals the externally applied contact load. Expressed in the dimensionless variables this condition reads:

$$\int_{-\infty}^{\infty} P(X,T)dX - \frac{\pi}{2} = 0 \quad \forall T \tag{5}$$

The equations (1)–(5) are discretized on a uniform grid with mesh size $\Delta_x$ extending over a domain $X_a \le X \le X_b$. Using second order central discretization for the poiseuille-term, first order upstream discretization for the wedge term, and first order backward discretization of the squeeze term, the approximation of Reynolds equation at time step $k$ in node $i$ reads:

$$\Delta_x^{-2}(\epsilon_{i-\frac{1}{2},k}P_{i-1,k} - (\epsilon_{i-\frac{1}{2},k} + \epsilon_{i+\frac{1}{2},k})P_{i,k} + \epsilon_{i+\frac{1}{2},k}P_{i+1,k}) - \Delta_x^{-1}(\bar{\rho}_{i,k}H_{i,k} - \bar{\rho}_{i-1,k}H_{i-1,k}) - \Delta_t^{-1}(\bar{\rho}_{i,k}H_{i,k} - \bar{\rho}_{i,k-1}H_{i,k-1}) = 0 \tag{6}$$

with the cavitation condition $P_{i,k} \ge 0$.

The discretized film thickness equation reads:

$$H_{i,k} = H_{0,k} + \frac{X_i^2}{2} + \Re(X_i, T_k) - \frac{1}{\pi}\sum_{j=1}^{n} K_{i,j}^{\Delta_x \Delta_x} P_{j,k} \tag{7}$$

where

$$K_{i,j}^{\Delta_x \Delta_x} = \left(i-j+\frac{1}{2}\right)\Delta_x\left(\ln\left(\left|i-j+\frac{1}{2}\right|\Delta_x\right) - 1\right) - \left(i-j-\frac{1}{2}\right)\Delta_x\left(\ln\left(\left|i-j-\frac{1}{2}\right|\Delta_x\right) - 1\right)$$

The dimensionless force balance equation reads after discretization:

$$\Delta_x \sum_{j=1}^{n-1} \frac{(P_{j,k} + P_{j+1,k})}{2} - \frac{\pi}{2} = 0 \quad \forall k \tag{8}$$

## 3 Numerical Solution

Before the dent reaches the position $X_d = X_a - 0.5\mathfrak{W}$, the squeeze term in the Reynolds equation will be almost zero in all nodes on the grid because of the large power in (4). Hence, film thickness and pressure profile are identical to the stationary smooth surface solution. An algorithm allowing fast and accurate calculation of this solution was presented in [8]. The algorithm is based on a combined Gauss-Seidel, Jacobi dipole relaxation scheme for solving the pressure from Reynolds equation whereas convergence of the process is accelerated using coarser grids, i.e. using Multilevel techniques. In addition, the computation of the elastic deformation integrals is accelerated using the same coarser grids. As a result, the computing time for the solution of the stationary problem is $O(n \ln n)$ if $n$ is the number of nodes on the grid. For details of the algorithm the reader is referred to [8].

From the moment the dent enters the domain the squeeze term will no longer be negligible. At each time step the pressure and film thickness are to be solved from Eqs. (6) to (8) using the solution of the previous time step for the evaluation of the squeeze term. When the trailing edge of the dent passes the exit boundary of the domain ($X_d \ge X_b + 0.5\mathfrak{W}$) the steady-state solution slowly returns.

**Table 1 Values of parameters and dimensionless parameters employed in the calculation**

| Parameter | Value | Dimension |
|---|---|---|
| $E'$ | $2.26 \cdot 10^{11}$ | [Pa] |
| $R$ | $1.4 \cdot 10^{-2}$ | [m] |
| $\alpha$ | $2.2 \cdot 10^{-8}$ | [$Pa^{-1}$] |
| $z$ | 0.68 | |
| $\eta_0$ | $40 \cdot 10^{-3}$ | [Pa s] |
| $p_h$ | $2.0 \cdot 10^{9}$ | [Pa] |
| $u_s$ | 1.97 | [$ms^{-1}$] |
| $b$ | $5.0 \cdot 10^{-4}$ | [m] |
| $\mathfrak{W}$ | 1.0 | |
| $\mathfrak{A}$ | 0.11 | |
| $M$ | 100 | |
| $L$ | 11.08 | |

The relaxation process solving the stationary problem is also suitable for the solution of the equations at each time step, provided the squeeze term is properly accounted for in the algorithm. Convergence of the process can be accelerated using the coarser grids. Hence, given a first approximation of the solution at a specific time step the equations can be solved by repeating coarse grid correction cycles until the desired accuracy has been obtained. The required number of cycles depends of course on the accuracy of the first approximation.

The most straightforward approach is to use the pressure profile of the previous time step as a first approximation to the solution on the current time step. Such an algorithm was, for example, employed by Woods et al. [9] when solving the dynamically loaded journal bearing problem. Hence, at each time step the coarser grids are only used to accelerate convergence of the relaxation process on the finest grid. The disadvantage of this technique is that the error in the first approximation at the finest grid contains all frequency components the grid can represent and at each time step the starting residual is rather large.

A more accurate first approximation, and consequently a reduction in the number of coarse grid correction cycles needed per time step, can be obtained if the coarser grids are employed in a way rather similar to the Full Multi Grid process for stationary problems. This alternative, the so-called $F$ cycle, was developed by Brandt and co-workers (see Appendix).

## 4 Results

The calculational results presented in this section apply to the conditions shown in Table 1. These conditions have been derived from a practical bearing application. Under these conditions the dimensionless parameters $\mathfrak{W} = 1$ and $\mathfrak{A} = 0.11$ describe a dent of 250 micrometer wide and 2 micrometer deep.

$M$ and $L$ are the Moes dimensionless load and materials parameter. They relate to the Dowson and Higginson parameters as:

$$M = W(2U)^{-1/2}$$
$$L = G(2U)^{1/4}$$

The solution has been calculated using some 200 time steps ($\Delta_t = 0.03125$) with 1409 nodes in spatial direction. Figure 2($a$) shows the steady-state solution at $T=0$ whereas Figs. 2($b$) to (2$d$) show the solutions at the times when $X_d = -0.5, 0.0, 0.5$, respectively.

For reasons of comparison Fig. 3 shows the solution for pressure and film thickness under steady-state conditions with the dent located in the center of the contact, i.e., at $X=0$.

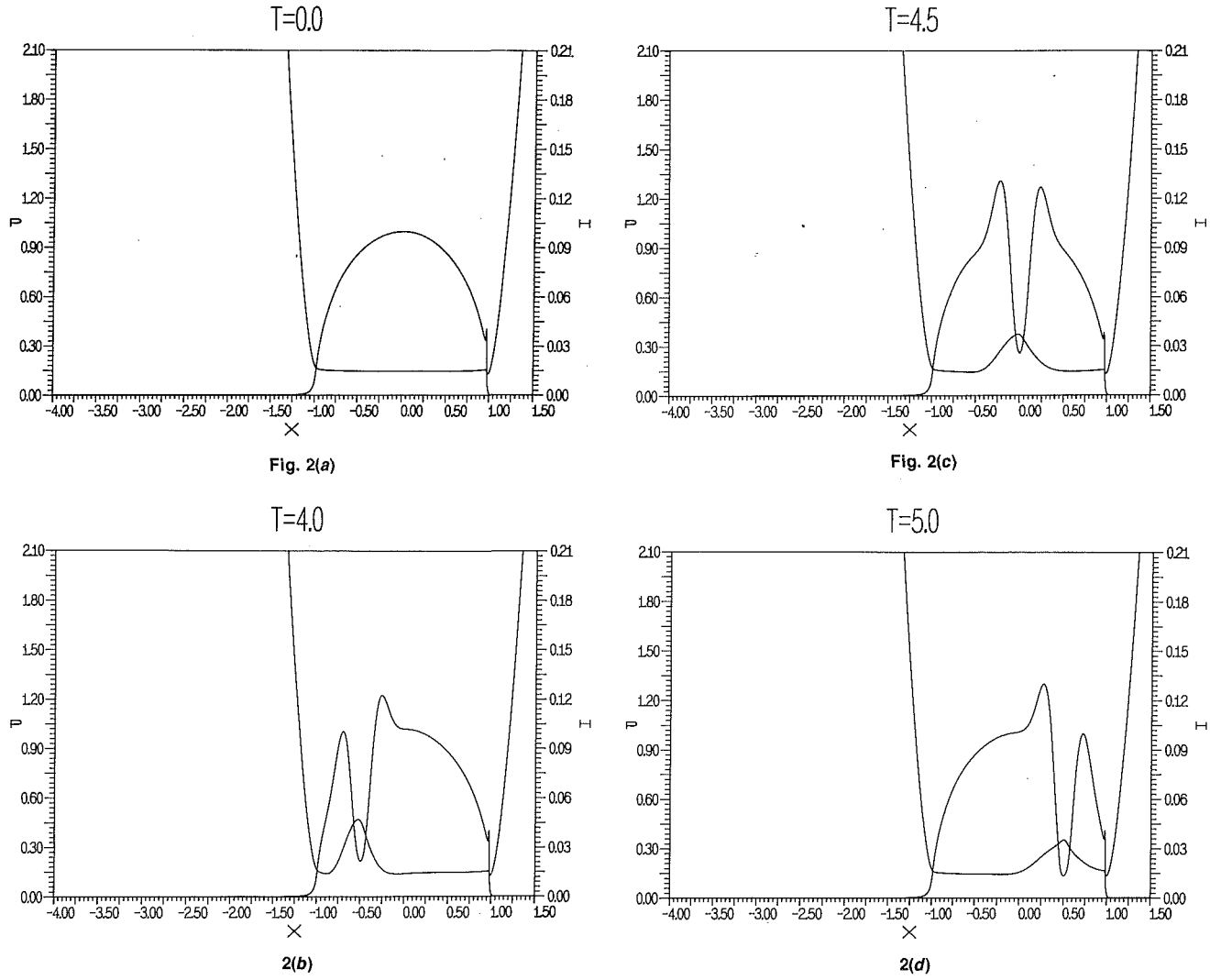


Fig. 2(*a*)

Fig. 2(*c*)

2(*b*)

2(*d*)

**Fig. 2 Solution $M=100$, $L=11.08$. Pressure and film thickness as a function of $X$. (*a*) Stationary solution. Transient solutions with dent at location: (*b*) $X_d=-0.5$, (*c*) $X_d=0.0$, (*d*) $X_d=0.5$.**

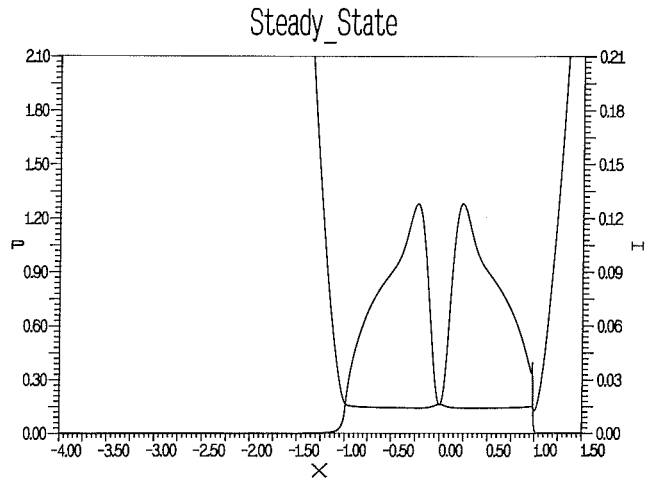


**Fig. 3 Stationary solution $M=100$, $L=11.08$ with dent at $X_d=0.0$. Pressure and film thickness as a function of $X$.**

Comparison of this steady-state solution with the transient solution shown in Fig. 2(*c*) clearly illustrates the effect of the squeeze term. Under steady-state conditions the Reynolds equation in the contact region reduces to:

$$\frac{d(\bar{\rho}H)}{dX}\approx 0 \tag{9}$$

Since Dowson and Higginson's equation limits the compressibility of the lubricant to about 30 percent, the result is a nearly uniform film thickness in the contact region that hardly deviates from the smooth surface solution. In the transient situation, however, because of the squeeze term, the change in dent geometry is much smaller. Furthermore, the pressure profile in Fig. 3 is almost symmetrical, the pressure rise at the trailing edge of the indentation equals the pressure rise at the leading edge. As can be seen from Fig. 2(*c*), in the transient situation the pressure rise at the trailing edge is larger whereas the pressure rise at the leading edge of the dent is smaller than it is in the steady state situation. These differences show the importance of the squeeze term, i.e. of the transient calculation.

An alternative way of presenting the results of the simulation is to monitor the pressure or film thickness at a certain point on one of the surfaces during its motion through the contact. As an example, the pressure variations experienced by two points at equal distance from the center of the dent are presented in Fig. 4(*a*). The curve on the left is for the point on the leading edge whereas the curve on the right is for the trailing edge. Both points are at a relatively large distance from the center of the dent, $|X_d-X|=0.5$. Note that these are exactly

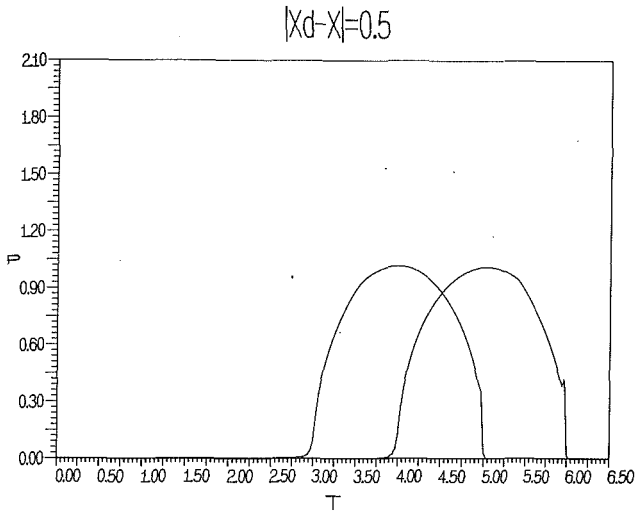


Fig. 4(*a*)

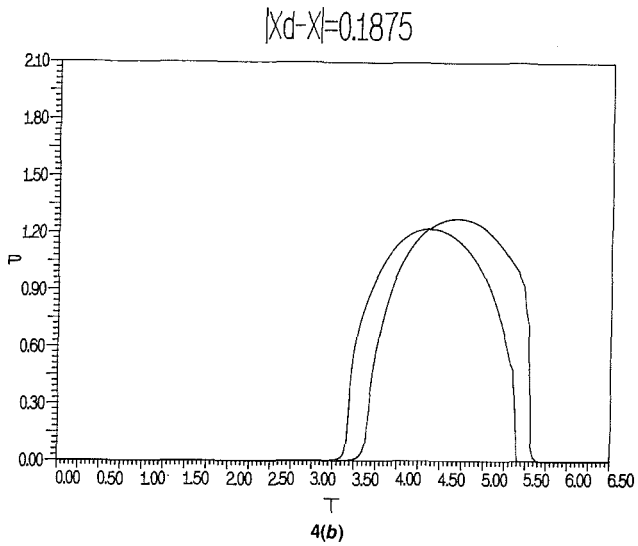


4(*b*)

**Fig. 4 Pressure as a function of $T$ for two points at location (*a*): $X_d - X = -0.5$ and $X_d - X = 0.5$, (*b*): $X_d - X = -0.1875$ and $X_d - X = 0.1875$ on the indented surface.**

the curves that a transducer on the surface at these locations would measure. Because they are relatively far removed from the center of the dent, both points experience a pressure signal over time that is equal to what any point would experience under smooth surface conditions. Similarly, Fig. 4(*b*) shows the pressure as a function of time for $|X_d - X| = 0.1875$, thus located closer to the center of the dent. In that case the maximum pressure experienced by the point at the trailing edge is obviously larger than the maximum pressure observed by the point at equal distance from the center of the dent on the leading edge.

To visualize this difference we define:

$$\mathcal{I}(X_d - X) = \int_0^{T_{\text{end}}} P(X_d - X, T)\, dT \tag{10}$$

to indicate the total "force" experienced by a point on the indented surface during overrolling. This integral is constant for points far removed from the dent. For pure rolling conditions this constant is $\pi/2$. For points in the vicinity of the dent the integral will deviate from this value. The value of the integral as a function of the distance from the center of the dent is presented in Fig. 5. This graph displays an interesting feature. Far from the center of the dent, the integral for a point on the leading edge equals the value of the integral for

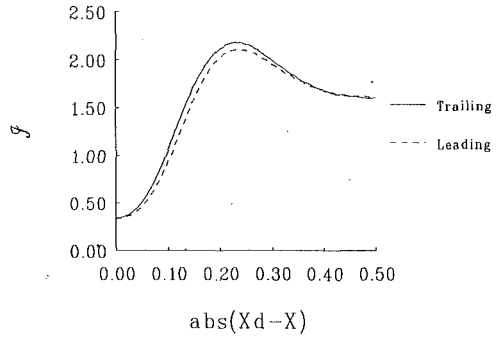


**Fig. 5 Value of integral $\mathcal{I}$ as a function of the distance from the center of the dent $|X_d - X|$ on the indented surface**

a point on the trailing edge. However, over the entire dent the integral for points on the trailing edge is larger than the integral for points on the leading edge. The maximum difference between the two curves is some 8 percent of the smooth surface value. Similar calculations have been carried out for smaller amplitudes giving the same overall results. However, in the case of a smaller amplitude the maximum difference between the two curves is also smaller. Hence, the maximum difference increases with increasing amplitude.

These results indicate that the maximum sub-surface stress experienced by points below the leading edge will be less than the maximum sub-surface stress experienced by points below the trailing edge; this is analyzed in detail in the next section.

## 5 Sub-Surface Stresses

The pressure distributions obtained in the previous sections can be applied to the study of fundamental tribological features like surface initiated fatigue. This phenomenon occurs when part of the contacting surfaces is damaged, either by incorrect manufacturing handling damage or by the overrolling of debris in the oil. These surface features will disturb the pressure in the lubricant film and consequently the stresses in the subsurface are affected. Generally, the surface imperfections can be viewed as local stress raisers, leading to imperfection-related fatigue failure and consequently a substantial reduction in service life.

A theoretical model to describe the relations between surface features and fatigue life is of great value since the experimental investigations are very time-consuming, energy-consuming and costly. The theoretical model used is described in detail in [10]. For this model to be accurate, the time-dependent behavior of the pressure in the lubricant film is essential, resulting in a time-consuming series of calculations (5 cpu hours on a SGI 240). As an example, the directional preference of fatigue initiation with respect to an indentation is discussed. Generally, a spall is created after (on the trailing edge of) the indentation. Using stationary lubricated or dynamic dry contact calculations, no preference in direction can be found. However, when the time-dependent lubricated calculations are performed an asymmetry in the pressure profile is observed (see Figs. 4 and 5). This difference is reflected in the sub-surface stresses, which are larger (and much closer to the surface) below the trailing edge of the indentation (see Fig. 6). Actually, the quantity displayed is not a stress, but a risk-related stress, incorporating the maximum shear stress over any angle, the hydrostatic pressure and the fatigue limit of the material (see [11]). For convenience we will briefly refer to it as a "stress."

This stress graph was obtained by computing the sub-surface stresses resulting from the pressure distribution at each time step. For this purpose the indented surface is monitored while the pressure profile is sweeping over it, and at each location in the material the maximum stress is recorded. It is obvious that far removed from the dent the iso-stress contours should

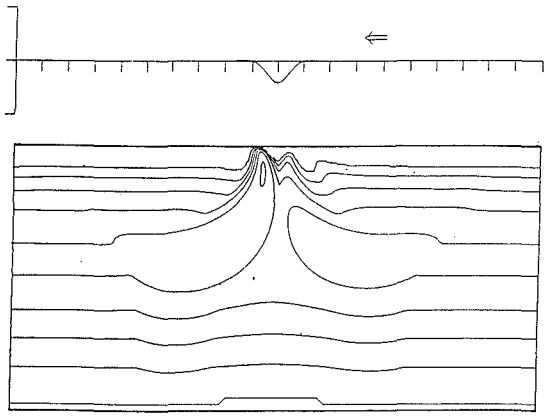

Fig. 6 Maximum sub-surface stresses below a dent during overrolling. Conditions as in Fig. 2.

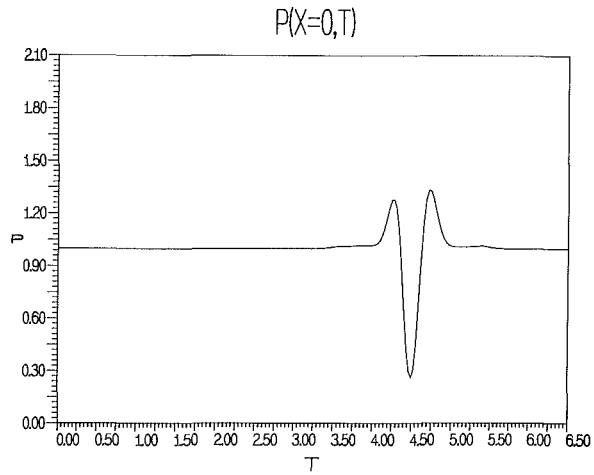


Fig. 7 Pressure in the center of the contact ($X=0$) as a function of $T$

become straight horizontal lines, only close to the dent will these contours be modified. Note that the stress concentration below the trailing edge of the dent is larger and extends much closer to the surface. As is explained in [10] the stresses can be converted to a (fatigue) risk integral. The risk integral over the left part of Fig. 6 is almost twice as high as the integral over the right part. Since the difference in stress is concentrated in a small region only (say 10 percent) the risk of spalling will be much higher for the trailing edge of the dent, explaining the experimentally observed preference. In real applications the depth of the indentations will be larger, and by extrapolation of the theoretical results obtained from shallower dents the asymmetry will be even more pronounced.

## 6 Condition Monitoring

As mentioned above surface indentations generally result in a significant reduction of the fatigue life of an EHL component. Because the unexpected breakdown of one of the bearings in a machine may have expensive consequences, the detection of surface defects, i.e. indentations, is an important topic in the condition monitoring of rolling bearings. One of the techniques employed is based on an analysis of the vibration signal. To a certain extent a simulation as presented above can provide some theoretical support for the research on this subject, in particular with respect to the relation between the indentation and its contribution to the vibration signal. For that purpose the pressure as a function of time is monitored at a certain location fixed in space. Figure 7 displays the pressure in the center of the contact as a function of time for the conditions and the surface feature considered in this paper. Before the leading edge of the dent reaches the specific location, and after the trailing edge passes the location the pressure equals the steady state value. The passage of the indentation causes a pressure variation and the frequency content of this variation is characteristic for its contribution to the vibrations in the bearing under the full film lubricated conditions assumed in this paper.

## 7 Conclusion

The overrolling of a surface indentation under realistic operating conditions was simulated. This simulation was carried out using a small time step and a large number of nodes in spatial direction. It was demonstrated that transient studies are essential in this type of research and that extrapolation of results from steady state conditions to practical conditions where both surfaces are moving is misleading. Also the subsurface stresses in the material were calculated. From the results it was concluded that spalling will most likely occur near the trailing edge of the indentation. The very same preference that has been found in experiments. Furthermore, a transient analysis as presented in this paper provides information that is of particular interest with respect to the condition monitoring of rolling bearings using vibration analysis.

Although strictly speaking the presented results only apply to line contact situations they will still give an accurate description of point contacts, where the Hertzian contact region is relatively wide. In the calculations a relatively shallow indentation was assumed. In practical situations the depth of the indentation is often much larger than 2 $\mu$m. In those situations cavitation will occur at the location of the indentation. Since pressure formation from a cavitated zone is not accounted for in this particular algorithm results for larger amplitudes were not presented. To simulate the overrolling of an indentation with a larger amplitude under these specific lubrication conditions an extension of the current algorithm is needed.

## Acknowledgment

The authors would like to thank Prof. H. Tijdeman of the Structural Mechanics Group for his stimulating interest. Part of the work was carried out in cooperation with Prof. A. Brandt during a stay at the Weizmann Institute of Science, Israel, sponsored by the Department of Mechanical Engineering of the University of Twente. The authors wish to thank Dr. H. H. Wittmeyer, Managing Director of the SKF Engineering & Research Center B.V., for his kind permission to publish this paper.

## References

Dowson, D., and Higginson, G. R., *Elasto-hydrodynamic Lubrication, the Fundamentals of Roller and Gear Lubrication*, Pergamon Press, Oxford, Great Britain, 1966.

Hamrock, B. J., and Dowson, D., "Isothermal Elastohydrodynamic Lubricant of Point Contacts, Part 1—Theoretical Formulation," ASME JOURNAL OF LUBRICATION TECHNOLOGY, Vol. 98, 1976, pp. 223-229.

Patir, N., and Cheng, H. S., "An Average Flow Model for Determining Effects of Three-Dimensional Roughness on Partial Hydrodynamic Lubrication," ASME JOURNAL OF TRIBOLOGY, Vol. 100, 1978, pp. 12-17.

Tripp, J. H., and Hamrock, B. J., "Surface Roughness Effects in Elastohydrodynamic Contacts," *Proc. 11th Leeds-Lyon Symposium on Tribology*, 1984, pp. 30-39.

Oh, K. P., "The Numerical Solution of Dynamically Loaded Elastohydrodynamic Contact as a Nonlinear Complementarity Problem," ASME JOURNAL OF TRIBOLOGY, Vol. 106, 1985, pp. 88-95.

Rong Tsong Lee, and Hamrock, B. J., "A Circular Non-Newtonian Fluid Model: Part 2—Used in Microelastohydrodynamic Lubrication," ASME JOURNAL OF TRIBOLOGY, Vol. 112, July 1990, pp. 497-505.

Chang, L., Cusano, C., and Conry, T. F., "Effects of Lubricant Rheology and Kinematic Conditions on Micro-Elastohydrodynamic Lubrication," ASME JOURNAL OF TRIBOLOGY, Vol. 111, 1989, pp. 344-351.

Venner, C. H., Ten Napel, W. E., and Bosma, R., "Advanced Multilevel

Solution of the EHL Line Contact Problem," ASME JOURNAL OF TRIBOLOGY, Vol. 112, 1990, pp. 426-432.

Woods, C. M., and Brewe, D. E., "The Solution of the Elrod Algorithm for a Dynamically Loaded Journal Bearing Using Multigrid Techniques," ASME JOURNAL OF TRIBOLOGY, Vol. 111, 1989, pp. 302-308.

Lubrecht, A. A., Venner, C. H., Lane, S., Jacobson, B., Ioannides, E., "Surface Damage—Comparison of Theoretical and Experimental Endurance Lives of Rolling Bearings," presented at Japan International Tribology Conference, Nagoya, Japan, 1990.

Ioannides, E., Jacobson, B. O., Tripp, J. H., "Prediction of Rolling Bearing Life Under Practical Operating Conditions," *Proc. 15th Leeds-Lyon Symposium on Tribology*, 1989, pp. 181-187.

## APPENDIX A

### The *F* Cycle

Consider the following discretized transient problem, where $L^{h,k}$ is a differential operator discretized on a grid with meshsize $h$, time step $k$, $u^{h,k}$ is the solution to be calculated, and $f^{h,k}$ is a right-hand side function:

$$L^{h,k}u^{h,k}=f^{h,k} \tag{11}$$

Using the solution at the previous time step $k-1$ as an approximation for the solution at the current time step $k$, residuals can be calculated according to:

$$R^{h,k}=f^{h,k}-L^{h,k}u^{h,k-1} \tag{12}$$

Defining:

$$\delta^{h,k}=u^{h,k}-u^{h,k-1} \tag{13}$$

Equation (11) can be written as:

$$L^{h,k}(u^{h,k-1}+\delta^{h,k})=L^{h,k}u^{h,k-1}+R^{h,k} \tag{14}$$

In general, $\delta^{h,k}$ contains all frequencies the grid can represent. In fact it is very often dominated by low frequencies. Using the normal FAS (Full Approximation Scheme) coarse grid correction cycle $O(\ln(n))$ cycles are needed to solve the problem to the level of the truncation error if $n$ is the number of nodes in spatial direction. If the first approximation would have been accurate up to the level of the truncation error on the coarser grid only $O(1)$ cycles would be needed. To obtain a first approximation of this accuracy is the purpose of the *F*-cycle.

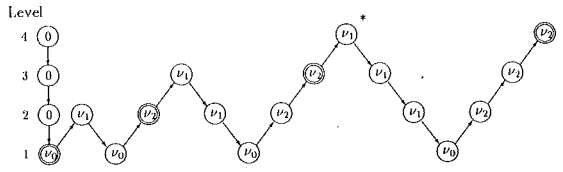


Fig. A.1

Characteristic for the *F*-cycle is that equation (14) is solved on the coarse grid first. Hence solving $\hat{u}^{H,k}$ from:

$$L^{H,k}(\hat{u}^{H,k})=L^{H,k}(I_h^H u^{h,k-1})+I_h^H R^{h,k} \tag{15}$$

an approximation $\tilde{u}^{h,k}$ is calculated according to:

$$\tilde{u}^{h,k}=u^{h,k-1}+I_H^h(\hat{u}^{H,k}-I_h^H u^{h,k-1}) \tag{16}$$

Subsequently, normal FAS coarse grid correction cycles can be used to reduce the error to the level of the truncation error. In case 1 $V(\nu_1, \nu_2)$ cycle is used, the solution process per time step is depicted in Fig. A.1 using 4 grids. The figures in the circles denote the number of relaxation sweeps carried out on the grid. Note that in the first coarsening sequence no (0) relaxations are performed. On the coarsest grid the equations should be solved nearly exactly. Hence, $\nu_0$ is in general larger than $\nu_1$ and $\nu_2$ which are in general $O(1)$. The double circles represent converged solutions. In this figure the first approximation to $u^{h,k}$ is marked by an $*$. This approximate solution is subsequently improved by additional cycles.